Downward migration of the zonal-mean circulation in the tropical atmosphere

Kevin DallaSanta[1,2,3], **Edwin P. Gerber**[1]

[1]Courant Institute of Mathematical Sciences, New York University, New York, New York, USA
[2]NASA Goddard Institute for Space Studies, New York, New York, USA
[3]Universities Space Research Association, Columbia, Maryland, USA

Key Points:

- Zonally coherent, or annular, fluctuations capture a higher fraction of circulation variability in the tropics than they do in midlatitudes
- Annular anomalies in tropical geopotential height and zonal wind migrate from the tropopause to the surface over approximately 10 days
- Downward migration is associated with a pulsing of the overturning Hadley circulation on subseasonal time scales

Corresponding author: Kevin DallaSanta, `kevin.dallasanta@nasa.gov`

Abstract

The annular modes of the extratropical atmosphere have received much attention for quantifying variability of the jet streams and storm tracks, despite the fact that the midlatitude circulation itself does not vary uniformly with longitude. While tropical fluctuations in geopotential height have lower amplitude than in the extratropics, they exhibit stronger zonal coherence, or dynamical annularity. A simple index is developed to characterize zonal-mean anomalies of the tropical circulation. It reveals that anomalies in geopotential height and zonal wind migrate downward from the upper troposphere to the surface on a time scale of about 10 days. These features are distinguishable from known modes of tropical variability, the Madden–Julian Oscillation in particular. Evidence from reanalysis and idealized model experiments confirms that this downward migration is quite generic and driven by mechanically forced variations in the strength of the Hadley circulation on subseasonal time scales.

Plain language summary: Earth's atmosphere has certain recurring patterns which are "annular," spanning an entire latitude circle. Annular patterns have proven to be surprisingly useful for weather and climate prediction. However, in the tropics, annular patterns have not been studied. We show that annular variability in the tropics does exist, and it contains interesting features that may be useful for prediction. In particular, anomalies in the circulation migrate downward from the tropopause (about 16 km) to the surface over 10 days. These features are also apparent in a relatively simple climate model, which helps direct further research.

1 Dynamical annularity of the atmospheric circulation

The annular modes of the extratropical circulation have received much attention for their predictive utility and dynamical insight (see Kushner, 2010, for an extensive review). They characterize atmospheric variability in a remarkable variety of contexts, from unforced intraseasonal variability (e.g., Thompson & Wallace, 1998; Feldstein, 2000) to forced responses associated with global warming (Thompson et al., 2000) or stratospheric ozone loss and recovery (Thompson et al., 2002). The designation "annular" refers to their zonally uniform structure, which characterizes an exchange of mass and momentum between the polar cap and midlatitudes (Thompson & Wallace, 2000), although their dynamics fundamentally depends on zonally asymmetric eddies (Hartmann & Lo, 1998).

From the time of their discovery, however, there has been much debate on the extent to which an annular mode, or midlatitude variability more generally, is actually annular. Deser et al. (2000) and Ambaum et al. (2001) observed that while variability of geopotential height becomes zonally uniform over the polar cap in a trivial sense, as the latitude circle approaches the scale of the deformation radius, variations in the midlatitudes are not at all zonally uniform.

More recently, Gerber & Thompson (2017) attributed the zonal structure of the annular mode patterns to the "statistical annularity" of the midlatitude circulation. The annularity of the pattern reflects the fact that the statistics of geopotential height variability are fairly uniform across longitudes, as opposed to the fluctuations themselves. They observed, however, that geopotential height variations in the tropics, while of weaker amplitude, exhibit far more zonal coherence.

The zonal coherence—or "dynamical annularity", to use the terminology of Gerber & Thompson (2017)—of geopotential height variability is quantified in Figure 1a. Here and throughout the study, data is daily and is taken from ERA–Interim reanalysis (Dee et al., 2011) from 1 January 1979 to 31 December 2017, with eddy statistics provided by Martineau et al. (2018). JRA–55 (Kobayashi et al., 2015) reanalysis yields nearly identical results (not shown).

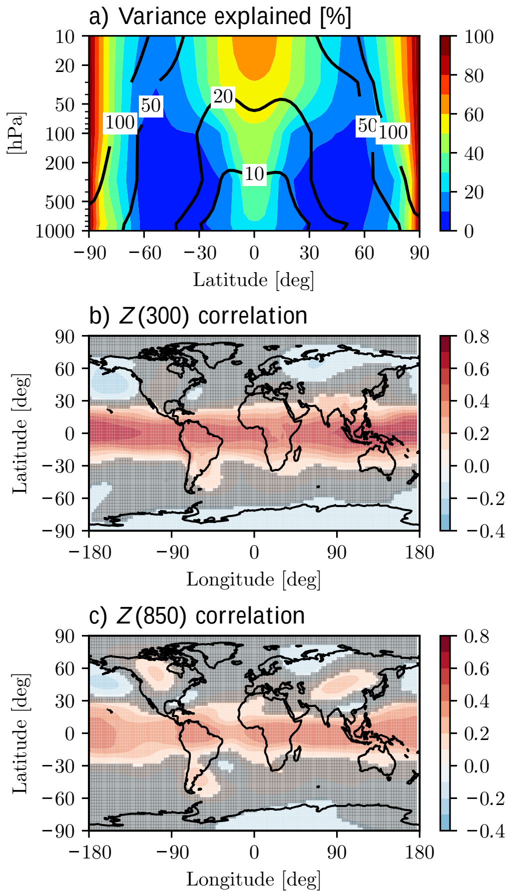

Figure 1. (a) The fraction of total variance associated with zonal mean anomalies in geopotential height (shaded), i.e., the power associated with wavenumber 0 in a zonal Fourier decomposition, normalized by the total power; and the RMS amplitude of the zonal mean flow (in meters; contoured). Here and throughout the text, unless specified otherwise, anomalies are defined as departures from a seasonally evolving climatology and highpass-filtered with a 1 year cutoff. (b) Correlation of 300 hPa geopotential height anomalies with our annular variability index $\overline{Z}$(300 hPa), described in the text. Hatching indicates regions where the correlation is not significantly different from 0 with 95% confidence, assuming a decorrelation time of 40 days to determine the degrees of freedom. (c) As in (b), but for the correlation of 850 hPa geopotential height anomalies with the $\overline{Z}$(850 hPa) index.

In the midlatitude troposphere—from 30 to 60 latitude in both hemispheres—less than 10% of variability is characterized by annular fluctuations. Near the poles, the geometry of the sphere naturally leads to a dominance of zonally coherent motion, but an additional maximum is observed in the tropics. Zonally coherent fluctuations of geopotential height characterize thus approximately a quarter of tropical variability at lower levels, the fraction increasing to almost a half at the tropopause. In this study, we investigate the structure of this zonal mean, or annular, variability in the tropical troposphere.

2 An index of zonal mean variability in the tropics

We first establish a convenient index to quantify annular variability in the tropics: zonal-mean geopotential height at the equator, computed on a given pressure level and denoted $\overline{Z}(p)$. We find that this simple index correlates very highly with more complex metrics, such as the leading time series from Principal Component Analysis of tropical geopotential height (cf. Baldwin & Thompson, 2009). Since these more complex options involve selecting parameters, we proceed with the simplest option. The data is filtered by subtracting the seasonal cycle and subsequently highpass-filtered with a 1-year cutoff to remove trends and low-frequency variability such as El Niño–Southern Oscillation (ENSO). As we discuss below, filtering is not critical.

Figure 1b,c shows the structure of variability associated with $\overline{Z}(850)$ and $\overline{Z}(300)$. The indices characterize broad variations across the entire tropics, extending approximately 20 from the equator, particularly in the Pacific sector which dominates the zonal mean. Broad correlation in geopotential reflects the weak rotation in the tropical atmosphere. In the weak temperature gradient limit (Sobel et al., 2001), any localized heating or cooling of the atmosphere (e.g., by convection) is balanced by ascent or descent, thereby homogenizing the temperature, and hence geopotential height. The enhanced positive correlation in Figure 1b relative to Figure 1c reflects the increase in annular variability with height shown in Figure 1a.

To characterize the zonal structure of variability, Gerber & Thompson (2017) suggest comparing single-point correlation maps in longitude, as shown in Figure S1. At lower levels, a given point is, on average, positively correlated with all other points around the latitude circle, the correlation decaying to zero towards the antipode. At upper levels, however, all points exhibit substantial positive correlation with others around the entire globe; at 300 hPa, the correlation is still approximately 0.4 at the antipode. This suggests that the zonal mean index characterizes broad variability at lower levels, albeit dominated by particular sectors at any given instant, which becomes increasing globally in nature in the upper troposphere. As a result, the zonal-mean index provides a convenient measure of large-scale variability across the tropics (Figure 1b,c), and capturing a substantial fraction of the total variability at all locations (Figure 1a).

3 Downward migration of annular circulation anomalies in the tropics

To explore the vertical coupling between zonal mean anomalies in geopotential height, Figure 2a shows the cross-correlation of $\overline{Z}(p)$ with $\overline{Z}(850)$. We begin with unfiltered data (from which only the annual cycle has been removed), but even in this raw reanalysis data, we see a downward migration of geopotential height anomalies from the upper troposphere to the surface on a time scale of about 10 days, followed by the hint of an opposite-signed anomaly which also migrates downward. A comparable picture emerges if we choose other levels (e.g., 300 hPa) as our base level of correlation.

Low-frequency variability (primarily ENSO) and trends lead to significant redness in the unfiltered cross-correlations. The subseasonal time scale becomes more apparent after applying a highpass filtering with 1 year cutoff (Figure 2b). This conservative approach to removing the red background of the unfiltered cross-correlations still allows in more than half of the variance at a time scale of 1 year, and reveals more clearly a downward-migrating signal, anticorrelated with preceding and proceeding anomalies. In testing we find that the results are not sensitive to the cutoff provided it is short enough to remove ENSO.

Several approaches to significance testing underscore the robustness of this phenomenon. Hatching in Figure 2 indicates statistical significance assuming a decorrelation time scale of 40 days, a conservative approach to estimating the effective degrees of freedom. Subsetting the dataset by decades leads to similar results, as does

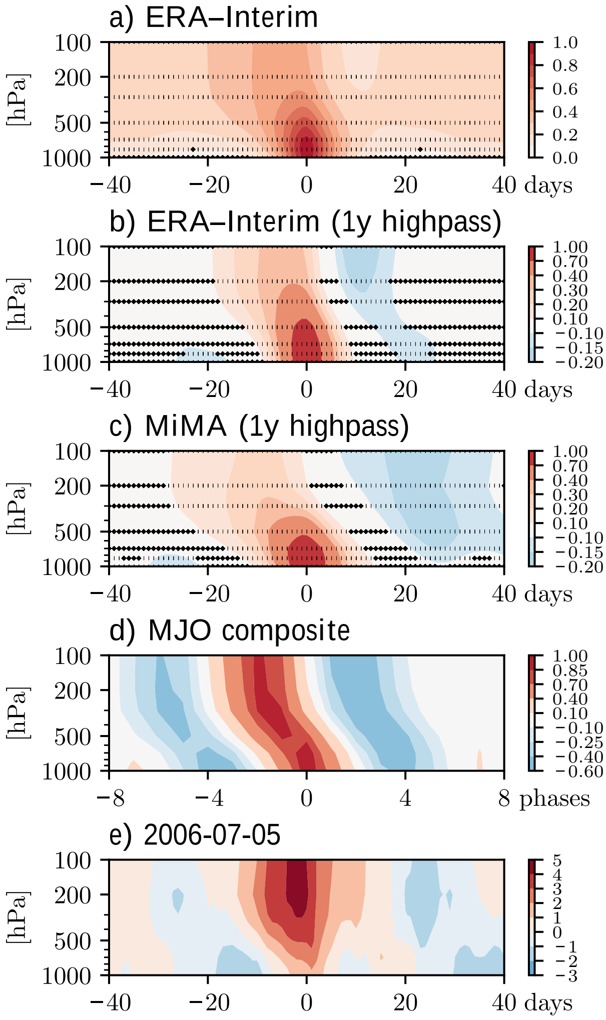

Figure 2. (a–d) Cross-correlation of $\overline{Z}(p)$ with $\overline{Z}(850)$. Data (a) from ERA–Interim unfiltered, (b) from ERA–Interim with a 1-year highpass filter, (c) from MiMA with a 1-year highpass filter, (d) composited by MJO RMM phase (amplitude-weighted; see text for details). (e) ERA–Interim $\overline{Z}(p)$ with a 1-year highpass filter, normalized to have unit variance, centered around July 5, 2006. In (a–c), hatching indicates inability to reject the null hypothesis that the correlation is zero with 95% confidence, using a decorrelation time of 40 days.

employing composites instead of cross-correlations (not shown). Significance will further be assessed dynamically and by comparing observations with a numerical model.

We first ask: is this downward migration simply the zonal mean manifestation of a known tropical mode of variability? Both the MJO (Andersen & Kuang, 2012) and ENSO (Seager et al., 2003) are known to exhibit zonally coherent variability. With respect to the latter, the high pass filtering in Figure 2b is one approach to removing the ENSO signal. (Alternatively, removing ENSO variability by regressing out the signal linearly correlated with the Niño 3.4 index yields a very similar result to Figure 2a). The highpass filter, however, will tend to amplify the relative importance of the MJO. To ensure the downward migration exists independently of the MJO, we repeated the analysis after regressing away variability linearly correlated with the principal components of the

Real-time Multivariate MJO (RMM) index (Wheeler & Hendon, 2004). Again, the results (not shown) are qualitatively identical with all MJO variability removed linearly.

As an additional approach to answering this question, we consider a numerical model which explicitly lacks ENSO or MJO-related variability. The Model of an Idealized Moist Atmosphere (MiMA; Jucker & Gerber, 2017) is an idealized aquaplanet, and modifications to the original model have been made to incorporate realistic zonal asymmetries in the lower boundary; a later iteration of this configuration has been published in Garfinkel et al. (2020). There is explicitly no oceanic variability and the model does not capture the MJO. The model has no cloud feedbacks and only resolves the large-scale circulation, employing a simplified parameterization of tropical convection.

Despite these substantial simplifications, geopotential anomalies also migrate downward in MiMA, on comparable temporal and vertical scales (Figure 2c). If anything, the cross-correlations in MiMA are slightly reduced in magnitude, implying that the full physics of the actual atmosphere act to strengthen the downward migration, rather than weaken it. Furthermore, the horizontal structure of tropical geopotential height variations in the model is comparable to Figure 1b,c (not shown).

We have shown idealized moist aquaplanet integrations because this is perhaps the simplest configuration that can reproduce the phenomenon. When one removes the impact of moisture from the model, as in the idealized atmospheric model of Held & Suarez (1994), the downward migration of geopotential anomalies is not apparent (not shown). Dry dynamical cores are fully capable of capturing the annular modes (e.g., Gerber & Vallis, 2007), or the more recently discovered Baroclinic Annular Modes (Barnes & Thompson, 2014), but our results indicate that additional complexity is critical to capturing the annular variations of the tropics.

Although the MJO is not necessary for the downward-migrating signal in equatorial geopotential height, it does exhibit a similar signal. To quantify the MJO's signature on zonal-mean geopotential, we construct weighted composites of normalized geopotential anomalies at each level as a function of RMM phase (Wheeler & Hendon, 2004). Noting that 8 phases of the oscillation correspond to approximately 40 days, these composites show qualitatively similar downward migration on consistent time scales (Figure 2d). While a pure traveling wave would not project on to the zonal mean, we interpret this signal to be associated with the growth and decay of MJO anomalies. Thus in isolation an MJO event is sufficient, but not necessary, to achieve downward migration.

Besides the MJO, might other tropical waves play a role in the zonal mean? Convectively coupled tropical waves are a source of variability that is absent in a dry dynamical core, but present in the real atmosphere and MiMA. This is a difficult hypothesis to probe quantitatively, as filtering of tropical waves is typically nonlinear due to pre-filtering of the red background (e.g., Wheeler & Kiladis, 1999). We have shown that subseasonal anomalies emerge from a red spectrum (Figure 2a,b).

There is some theoretical evidence that zonally symmetric variability could also drive vacillations. Zhao & Ghil (1991) investigated symmetric inertial instability in a zonally averaged two-layer model and found a solution with zonal mean oscillations in geopotential shear. However, further investigation is needed to bridge their idealized study with observational data. In particular, our analysis indicates that eddy momentum fluxes also fluctuate coherently (Section 4), which suggests a pathway for waves to impact the zonal mean.

To get a sense of the actual variability, an example of downward migration for both positive and negative anomalies in the reanalysis record is shown in Figure 2e. The vertical coherence and time scales of these events are similar to the mean cross-correlated picture.

These events and the cross-correlated average are reminiscent of the "dripping paint plots" of extratropical annular mode composites (Baldwin & Dunkerton, 2001), although the resemblance is superficial, as the dynamics of the two are quite distinct. Downward migration in the Northern and Southern annular mode indices involves coupling between the tropospheric extratropical jet and the stratospheric polar vortex: a deceleration of the polar vortex is usually followed by a nearly barotropic response in the troposphere (Thompson & Wallace, 2000; Baldwin & Dunkerton, 2001). In the tropics, the downward migration is entirely within the troposphere. In addition, downward migration in the extratropical annular modes, while very robust, only appears in composite analysis and is not evident from simple cross-correlation, unlike the tropical variability explored here.

Longitude–height cross-sections of geopotential height at key lags are shown in Figure S2 (left column) to characterize the zonal structure of the downward migration. Fluctuations of the zonal mean are positively correlated with individual points at all longitudes, but an additional wave-1 structure indicates enhanced activity over the Indo–Pacific as observed in Figure 1b,c. Similar coherence of geopotential height in longitude and height are also observed with the 2006-07-05 event (Figure S2, right column), albeit with additional variability on synoptic scales.

Downward migration in the tropical circulation is also apparent in other meteorological variables, as shown in cross correlation of the zonal mean zonal wind with $\overline{Z}(850)$ in Figure 3a. Weakened trade winds migrate downward in association with anomalously high geopotential height, reflecting cyclostrophic balance. Conversely, strengthened trade wind anomalies migrate downward in concert with negative geopotential height anomalies. In the next section, we parse the structure of downward migrating geopotential and zonal wind by cross-correlating with the key dynamical fields at play.

4 Mechanically forced variations in the Hadley Circulation

Geopotential height is the altitude of a given pressure surface of the atmosphere, and thus depends on both the surface pressure and the temperature of the atmosphere below. A pressure surface is elevated when the surface pressure increases; that is, when the local mass of the atmospheric column is increased, requiring one to ascend higher through the atmosphere to reach a given pressure. Similarly, a pressure surface is elevated if the atmosphere below it is warmer, and so less dense, again requiring a higher ascent to reach a given pressure. The downward migration of geopotential height anomalies shown in Figure 2 thus corresponds to a coordination, or phase locking, between temperature anomalies and surface pressure anomalies in the tropics.

Figure 3b,c show that anomalously high low-level geopotential (or surface pressure) is preceded by anomalously warm temperatures throughout the tropical troposphere, which lifts geopotential height at upper levels. Correlation between low-level geopotential and temperature reaches a maximum at a lead of 10 days (10 on the horizontal axis), at which time surface pressure anomalies are uncorrelated: the atmosphere is warmest when surface pressure is neutral. The atmosphere cools as surface pressure anomalies build, with temperature anomalies vanishing at lag 0, just as surface pressure reaches a maximum. The atmosphere continues to cool, as surface pressure relaxes, reaching a maximum negative anomaly near a lag of 10 days (10 on the horizontal axis), maintaining quadrature with the surface pressure field.

Since the surface pressure indicates the total mass of the atmospheric column, downward migration in tropical geopotential can thus be described as a progression from *hot* to *heavy* (more mass) to *cold*. The cross-correlation is symmetric, by construction, but additional testing via composite analysis (not shown) reveals that this symmetry does

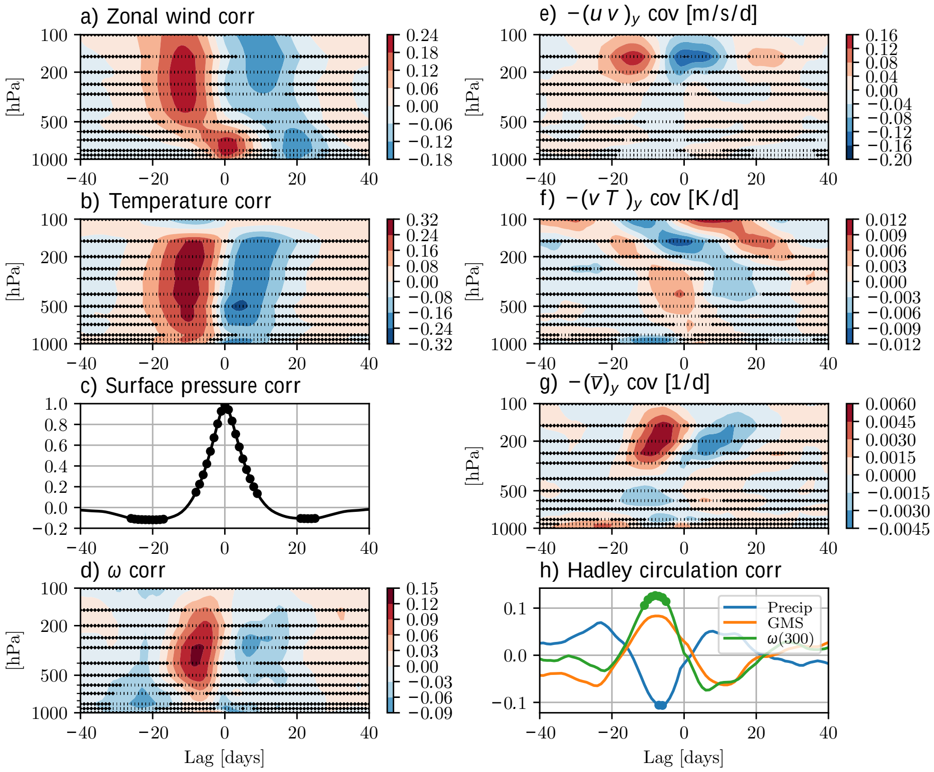

Figure 3. Cross-correlation and covariance of normalized $\overline{Z}(850)$ with anomalous zonally averaged equatorial (a) temperature, (b) zonal wind, (c) surface pressure p_s, (d) pressure velocity !, (e) eddy momentum flux convergence, (f) eddy temperature flux convergence, (g) meridional wind convergence, and (h) Hadley circulation metrics. Panels (a–d) and (h) are correlations; panels (e–g) are shown as the covariance to give the dynamical tendencies physical units which can be compared across pressure levels. In (h), the Hadley circulation is characterized by precipitation rate (Precip), gross moist stability (GMS; moist static energy at 850 hPa minus 200 hPa), and vertical velocity ! at 300 hPa. Hatching and missing dots indicate the inability to reject the null hypothesis at 95% confidence. We have assumed a conservative decorrelation time scale of 40 days for the more persistent fields in (a–c) and (h), as in previous figures. The decorrelation scale of eddy fluxes, !, and v_y is much shorter, on the order of days. For (d–g), we have therefore assumed a time scale of 10 days.

hold between positive and negative anomalies: downward migration of negative geopotential height anomalies are associated with a cold–light–warm pattern.

This phase locking between temperature and surface pressure reflects a common dynamical origin: a pulsing of the Hadley circulation, seen in the vertical (pressure) velocity in Figure 3d and other metrics in Figure 3h. The positive correlation between the pressure velocity ! and temperature, however, indicates that the anomalies must be mechanically forced: warmer temperature is associated with anomalous downwelling. For thermodynamic forcing to create kinetic energy, warm air must rise. This suggests that the temperature tendency is more attributable to the anomalous downwelling, which reduces the overall adiabatic cooling by the ascending branch of the Hadley Circulation. We also observe a concomitant reduction in precipitation in Figure 3h, suggesting that the temperature anomalies are not being forced by enhanced latent heating. The reduction in precipitation is consistent with increase in gross moist stability associated with warming of the free troposphere.

The dynamical origin of the vacillation can be traced back to anomalous eddy-driven momentum convergence in the upper troposphere at a lead time of 16 to 20 days relative to the $\overline{Z}(850)$ index, as seen in Figure 3e. The eddy forcing can be characterized by the divergence of the momentum flux at the equator, which reflects a broad anomaly in momentum forcing across the tropics, as shown in the meridional cross-section of the momentum flux at a lead of 16 days in Figure 4a. This positive anomaly reflects a weakening of the climatological momentum flux out of the tropics, which drives the downwelling anomaly peaking at a lead of 8 days (Figure 3d) as in the eddy-driven pump mechanism of Holton et al. (1995). Strictly speaking, this mechanism cannot be applied at the equator, but the momentum flux anomaly is spread over the tropics (Figure 4a). Momentum fluxes out of the Hadley circulation allow flow across angular momentum surfaces, enhancing the thermodynamically driven cell. A weakening of momentum flux leads to a temporary slowdown of the circulation, particularly at upper levels, which can be inferred from the convergence of the meridional velocity (v_y), shown in Figure 3g.

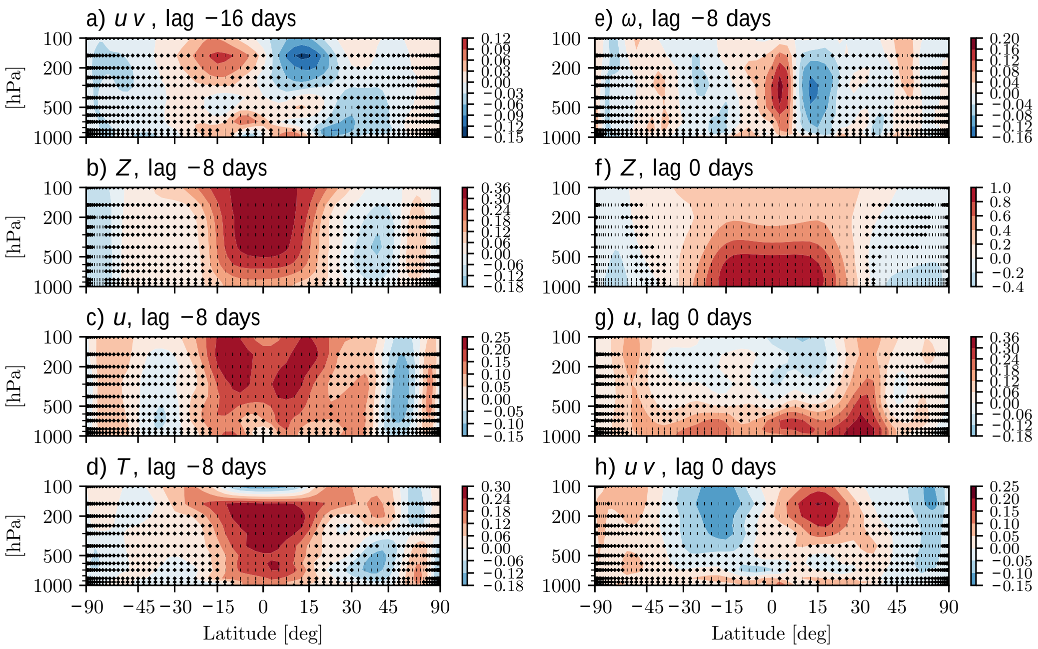

Figure 4. Cross-correlations of $\overline{Z}(850)$ with zonal mean fields as a function of latitude (degrees) and height (hPa) at varying lead/lag times: (a) eddy momentum flux (lag −16 days), (b) geopotential height (−8 days), (c) zonal wind (−8 days), (d) temperature (−8 days), (e) pressure velocity (−8 days), (f) geopotential height (0 days), (g) zonal mean wind (0 days), and (h) eddy momentum flux (0 days). As before, fields are climatological anomalies and highpass-filtered with a cutoff of 1 year. Negative lags indicate that the specified field leads $\overline{Z}(850)$. Statistical significance is assessed as in Figure 3: 40 days for (b,c,d,f,g), and 10 days for (a,e,h).

At a lead time of 8 days, broad anomalies in geopotential and temperature anomalies are observed throughout the tropics, extending 20 into each hemisphere, as shown in the meridional cross-sections in Figure 4b,c. Anomalies in the trade winds peak off the equator, near 10 N and S. The pressure velocity field at the same time, shown in Figure 4b, exhibits more fine scale structure. A reduction of upwelling (positive !) is observed within 10° of the equator in both hemispheres, but the correlation is stronger in the Northern Hemisphere. Anomalous upwelling is observed polewards of 10°, again, more significantly in the boreal hemisphere. This suggests that a simple reduction in adiabatic expansion driven by the reduction of upwelling cannot explain the meridional temperature structure. A detailed budget is the subject of further analysis, but we find that the eddy temperature flux (Figure 3f) generally acts to damp the temperature anomalies, although it exhibits evidence of a signal extending higher into the stratosphere.

Figure 4f,g,h shows the correlation of anomalies of zonal mean geopotential height, wind, and eddy momentum flux, concomitant with maximum positive anomalies of $\overline{Z}(850)$. As seen in Figure 2, geopotential height anomalies have descended toward the surface across the tropics from 20° S to 20° N, peaking at levels below 500 hPa, and associated with low level trade wind anomalies that extend further into the extratropics. Eddy momentum flux anomalies have flipped sign relative to earlier lags, driving the subsequent propagation of opposite anomalies in height and wind at positive lags, essentially repeating the same cycle, but with opposite sign.

Lastly, it is important to account for the surface pressure anomalies, which are essential to the downward propagating signal. The slowdown of the circulation before lag 0 also enhances mass convergence over the equator, focused at upper levels where the tropospheric branch of the Hadley circulation diverges (Figure 3g). This accounts for the surface pressure fluctuations, as the meridional contribution to the surface pressure tendency is (in pressure coordinates):

$$\frac{\partial \overline{p}_s}{\partial t} = -\frac{\partial}{\partial y}\overline{\int_0^{p_s} v\,\mathrm{d}p} = -\int_0^{\overline{p}_s} \frac{\partial \overline{v}}{\partial y}\,\mathrm{d}p - \overline{v(p_s)\frac{\partial p_s}{\partial y}} - \overline{\int_{\overline{p}_s}^{p_s} \frac{\partial v'}{\partial y}\,\mathrm{d}p}. \tag{1}$$

The zonal average tendency is dominated by the vertical integral of $-\overline{v}_y$ (the first term on the RHS) as mass convergence is occurring at upper levels, rather than at the lower boundary (the second and third terms on the RHS). The convergence of mass is consistent with the slowdown in the circulation driven by momentum fluxes, peaking in the upper half of the atmosphere where the momentum forcing is strongest.

We acknowledge that cross-correlation analysis does not indicate causation, and that the signals presented in Figures 3 and 4 are weak relative to background noise, i.e., the abundance of tropical processes that survive the 1-year high pass filter. More aggressive filtering increases the magnitude of the correlation (not shown), but we have taken a conservative filtering approach to avoid artificially amplifying variability on subseasonal timescales. Our confidence in the mechanism rests primarily on the dynamical consistency between the eddy forcing and zonal mean circulation eddies, taken together. It is an open question as to what drives the anomalous eddy forcing that triggers the cycle, and further research is required to untangle the role of tropical and extratropical wave sources.

5 Summary

Annular variations in geopotential height capture a higher fraction of the natural variability in the tropical atmosphere as compared to the midlatitudes. We constructed a simple index to characterize the annular variability of the tropics: zonal-mean geopotential at the equator. The index tracks broad variations of the height fields at each level, extending approximately 20 degrees in latitude into both hemispheres. Cross-correlation between levels reveals downward-migrating circulation anomalies on intraseasonal time scales. Positive geopotential height anomalies, associated with decreased trade winds, migrate from the tropopause to the surface on a time scale of approximately 10 days. Likewise, enhanced trade winds migrate downward with negative geopotential height anomalies.

While the Madden–Julian Oscillation (MJO) is associated with a similar zonal mean signature, we find that these downward migration circulation anomalies are more generic.

They reflect a phase locking of temperature and surface pressure anomalies associated with variations in the overturning circulation on subseasonal time scales. Anticorrelation between the vertical velocity and temperature indicates that these variations are mechanically driven, consistent with anomalies in eddy momentum flux convergence. Simulations with idealized atmospheric models attest to the generic nature of these downward migrating anomalies, but indicate that the mechanism depends on the presence of tropical variability. Future work intends to explore the mechanism in greater detail, and investigate the predictability of these oscillations.

Acknowledgments

We thank Olivier Pauluis, David Thompson, and an anonymous reviewer for helpful discussion and feedback on earlier versions of this manuscript. This research was supported by the NSF through grant AGS-1852727 to New York University. KD also acknowledges support from the NASA Postdoctoral Program at the Goddard Institute for Space Studies.

Data availability. This study is based on atmospheric reanalyses and integrations with an idealized model atmospheric model. ERA–Interim reanalysis was obtained from ECMWF at `https://apps.ecmwf.int/datasets/` and is documented by (Dee et al., 2011). Eddy statistics derived from ERA–Interim were provided by Martineau et al. (2018), available at `https://catalogue.ceda.ac.uk/`. Key results were checked with JRA-55 reanalysis (not shown), available and documented at `https://jra.kishou.go.jp/JRA-55/index_en.html`. MiMA is documented by Jucker & Gerber (2017) and Garfinkel et al. (2020). The source code and run parameters for the original MiMA model are available at `https://github.com/mjucker/MiMA`, and the modified configuration at `https://doi.org/10.5281/zenodo.1401407`.

References

Ambaum, M. H., Hoskins, B. J., & Stephenson, D. B. (2001). Arctic Oscillation or North Atlantic Oscillation? *Journal of Climate*, *14*(16), 3495–3507.

Andersen, J. A., & Kuang, Z. (2012). Moist static energy budget of MJO-like disturbances in the atmosphere of a zonally symmetric aquaplanet. *Journal of Climate*, *25*(8), 2782–2804.

Baldwin, M. P., & Dunkerton, T. J. (2001). Stratospheric Harbingers of Anomalous Weather Regimes. *Science*, *294*(5542), 581–584.

Baldwin, M. P., & Thompson, D. W. (2009). A critical comparison of stratosphere–troposphere coupling indices. *Quarterly Journal of the Royal Meteorological Society*, *135*(644), 1661–1672.

Barnes, E. A., & Thompson, D. W. (2014). Comparing the roles of barotropic versus baroclinic feedbacks in the atmospheres response to mechanical forcing. *Journal of the Atmospheric Sciences*, *71*(1), 177–194.

Dee, D. P., Uppala, S. M., Simmons, A. J., Berrisford, P., Poli, P., Kobayashi, S., ... Geer, A. J. (2011). The ERA-Interim reanalysis: configuration and performance of the data assimilation system. *Q. J. R. Meteorol. Soc.*, *137*, 553–597.

Deser, C., Walsh, J. E., & Timlin, M. S. (2000). Arctic sea ice variability in the context of recent atmospheric circulation trends. *Journal of Climate*, *13*(3), 617–633.

Feldstein, S. B. (2000). The timescale, power spectra, and climate noise properties of teleconnection patterns. *Journal of Climate*, *13*(24), 4430–4440.

Garfinkel, C. I., White, I., Gerber, E. P., Jucker, M., & Erez, M. (2020). The building blocks of northern hemisphere wintertime stationary waves. *Journal of Climate*(2020).

Gerber, E. P., & Thompson, D. W. J. (2017). What Makes an Annular Mode Annular? *Journal of the Atmospheric Sciences*, *74*(2), 317–332.

Gerber, E. P., & Vallis, G. K. (2007). EddyZonal Flow Interactions and the Persistence of the Zonal Index. *J. Atmos. Sci.*, *64*(9), 3296–3311.
Hartmann, D. L., & Lo, F. (1998). Wave-driven zonal flow vacillation in the southern hemisphere. *Journal of the Atmospheric Sciences*, *55*(8), 1303–1315.
Held, I. M., & Suarez, M. J. (1994). A Proposal for the Intercomparison of the Dynamical Cores of Atmospheric General Circulation Models. *Bull. Am. Meteorol. Soc.*, *75*(10), 1825–1830.
Holton, J. R., Haynes, P. H., Mcintyre, M. E., Douglass, A. R., & Rood, B. (1995). Stratosphere-Troposphere Exchange. *Rev. Geophys.*, *33*(4), 403–439.
Jucker, M., & Gerber, E. P. (2017). Untangling the annual cycle of the tropical tropopause layer with an idealized moist model. *J. Clim.*, *30*(18), 7339–7358.
Kobayashi, S., Ota, Y., Harada, Y., Ebita, A., Moriya, M., Onoda, H., ... Kiyotoshi, T. (2015). The JRA-55 reanalysis: General specifications and basic characteristics. *Journal of the Meteorological Society of Japan*, *93*(1), 5–48.
Kushner, P. J. (2010). Annular modes of the troposphere and stratosphere. *Geophysical Monograph Series*, *190*(1), 59–91.
Martineau, P., Wright, J. S., Zhu, N., & Fujiwara, M. (2018). Zonal-mean data set of global atmospheric reanalyses on pressure levels. *Earth System Science Data*, *10*(4), 1925–1941.
Seager, R., Harnik, N., Kushnir, Y., Robinson, W., & Miller, J. (2003). Mechanisms of hemispherically symmetric climate variability. *Journal of Climate*, *16*(18), 2960–2978.
Sobel, A. H., Nilsson, J., & Polvani, L. M. (2001). The Weak Temperature Gradient Approximation and Balanced Tropical Moisture Waves. *Journal of the Atmospheric Sciences*, *58*(23), 3650–3665.
Thompson, D. W. J., Solomon, S., & Hill, L. (2002). Interpretation of Recent Southern Hemisphere Climate Change. *Science*, *296*(5569), 895–899.
Thompson, D. W. J., & Wallace, J. M. (1998). The arctic oscillation signature in the wintertime geopotential height and temperature fields. *Geophysical research letters*, *25*(9), 1297–1300.
Thompson, D. W. J., & Wallace, J. M. (2000). Annular Mode in the Extratropical Circulation. Part I : Month-to-Month Variability. *J. Clim.*, *13*(1999), 1000–1016.
Thompson, D. W. J., Wallace, J. M., & Hegerl, G. C. (2000). Annular modes in the extratropical circulation. part ii: Trends. *Journal of climate*, *13*(5), 1018–1036.
Wheeler, M., & Hendon, H. H. (2004). An all-season real-time multivariate mjo index: Development of an index for monitoring and prediction. *Monthly weather review*, *132*(8), 1917–1932.
Wheeler, M., & Kiladis, G. N. (1999). Convectively coupled equatorial waves: Analysis of clouds and temperature in the wavenumber–frequency domain. *Journal of the Atmospheric Sciences*, *56*(3), 374–399.
Zhao, J. X., & Ghil, M. (1991). Nonlinear Symmetric Instability and Intraseasonal Oscillations in the Tropical Atmosphere. *Journal of the Atmospheric Sciences*, *48*(24), 2552–2568.

Supplemental figures

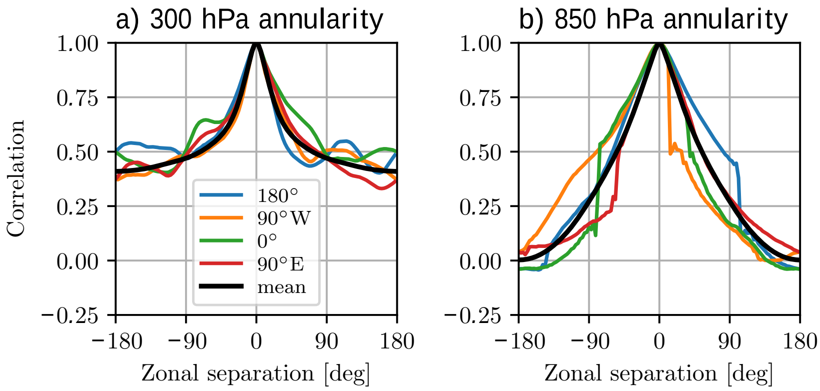

Figure S1. Pairwise correlation between geopotential height anomalies on the equator as a function of longitudinal separation at (a) 300 and (b) 850 hPa. Explicitly, this is: corr ($Z_{\ 0}; Z_{\ 0+\Delta}$), for four base longitudes $_0$ (indicated by the legend) as a function of zonal separation Δ in degrees longitude. As explored by Gerber & Thompson (2017), this allows one to compare the correlation structure in different sectors. The black line is the mean of the correlation maps over all longitudes (not just the four points shown). As with the analysis in the main text, anomalies are climatological and highpass-filtered with a cutoff of 1 year. The abrupt drops and kinks in correlation at 850 hPa are associated with orography at the equator.